

Fluid pressure changes recorded by trace elements in quartz

Hugues Raimbourg, Vincent Famin, Aurélien Canizarès, Emmanuel Le Trong

▶ **To cite this version:**

Hugues Raimbourg, Vincent Famin, Aurélien Canizarès, Emmanuel Le Trong. Fluid pressure changes recorded by trace elements in quartz. Geochemistry, Geophysics, Geosystems, 2022, 10.1029/2022GC010346 . insu-03774743

HAL Id: insu-03774743

https://insu.hal.science/insu-03774743

Submitted on 12 Oct 2022

HAL is a multi-disciplinary open access archive for the deposit and dissemination of scientific research documents, whether they are published or not. The documents may come from teaching and research institutions in France or abroad, or from public or private research centers.

L'archive ouverte pluridisciplinaire **HAL**, est destinée au dépôt et à la diffusion de documents scientifiques de niveau recherche, publiés ou non, émanant des établissements d'enseignement et de recherche français ou étrangers, des laboratoires publics ou privés.



Distributed under a Creative Commons Attribution - NonCommercial - NoDerivatives 4.0 International License

Check for updates

Geochemistry, Geophysics, Geosystems®

AGU ADVANCING EARTH AND SPACE SCIENCE

15252027, 2022, 10, Downloaded from https://agupubs.onlinelibrary.wiley.com/doi/10.1029/2022GC010346 by Portail BibCNRS INSU, Wiley Online Library on [12/10/2022]. See the Terms and Conditions (https://onlinelibrary.wiley.com/terms-and-conditions) on Wiley Online Library for rules of use; OA articles are governed by the applicable Creative Commons License

RESEARCH LETTER
10.1029/2022GC010346

Fluid Pressure Changes Recorded by Trace Elements in Quartz

Hugues Raimbourg[1], Vincent Famin[2,3], Aurélien Canizarès[4], and Emmanuel Le Trong[1]

[1]Institut des Sciences de la Terre d'Orléans, UMR 7327, CNRS, BRGM, Université d'Orléans, Orléans, France, [2]Université de Paris, Institut de Physique du Globe de Paris, CNRS, Paris, France, [3]Université de La Réunion, Laboratoire GéoSciences Réunion, Saint Denis, France, [4]CEMHTI, CNRS, Orléans, France

Key Points:

- In low-temperature hydrothermal quartz, trace element concentration and fluid pressure are correlated
- High aluminum concentrations are observed in domains where out-of-equilibrium and rapid growth of quartz occurred under low fluid pressure
- The variations in aluminum content are controlled by variations in fluid pressure during the seismic cycle

Supporting Information:

Supporting Information may be found in the online version of this article.

Correspondence to:

H. Raimbourg,
hugues.raimbourg@univ-orleans.fr

Citation:

Raimbourg, H., Famin, V., Canizarès, A., & Le Trong, E. (2022). Fluid pressure changes recorded by trace elements in quartz. *Geochemistry, Geophysics, Geosystems*, *23*, e2022GC010346. https://doi.org/10.1029/2022GC010346

Received 20 JAN 2022
Accepted 9 MAY 2022

Author Contributions:

Conceptualization: Hugues Raimbourg, Vincent Famin
Investigation: Hugues Raimbourg, Vincent Famin
Methodology: Hugues Raimbourg, Vincent Famin, Aurélien Canizarès, Emmanuel Le Trong
Software: Emmanuel Le Trong
Writing – original draft: Hugues Raimbourg, Vincent Famin
Writing – review & editing: Hugues Raimbourg, Vincent Famin

© 2022 The Authors.
This is an open access article under the terms of the Creative Commons Attribution-NonCommercial License, which permits use, distribution and reproduction in any medium, provided the original work is properly cited and is not used for commercial purposes.

Abstract Fluid pressure is a key parameter in earthquake mechanics, controlling seismic failure and plate coupling in convergent zones. Yet fluid pressure is also extremely difficult to quantify at seismogenic depth, which limits our knowledge of the stress state in accretionary prisms. Here, we show that the geochemical record of exhumed hydrothermal quartz veins may be used to place quantitative bounds on fluid pressure variations in subduction zones. The studied veins come from sediments accreted and exhumed by plate convergence in southwestern Japan. Quartz in veins displays growth rims of contrasted bright blue/dark brown cathodoluminescence (CL) colors, high/low Al concentrations, and low/high fluid inclusion abundance. Because Si-Al substitution (and charge compensation by Li) strongly depends on the rate of quartz precipitation and Si solubility, Al-Li concentrations must be sensitive to fluid pressure. This is confirmed by fluid inclusions, the density of which, converted into trapping pressures, record fluid pressure drops by up to ~70 MPa from CL-brown, Al-Li-poor rims to CL-blue, Al-Li-rich quartz rims. CL-blue rims grow at a fast rate, high Si supersaturation and low fluid pressure whereas CL-brown rims grow at a slower pace, lower Si supersaturation, and higher fluid pressure. Quartz trace element chemistry thus offers a promising tool to quantify deep fluid pressure variations and their relationships to earthquakes.

Plain Language Summary Rocks at depth contain a small proportion of cavities filled with a fluid. The pressure of this cavity-filling fluid plays a major role in earthquakes generation. Nonetheless, measuring fluid pressure at depth is extremely difficult. One method relies on the analysis of fluid inclusions trapped at depth, but it is plagued by the possible modifications of their properties (i.e., their reequilibration) during exhumation. In this study we have conjointly analyzed, in japanese deformation zones, methane-rich fluid inclusions and the chemical composition of their quartz crystal hosts, which grew contemporaneously. We observed, in the quartz, growth rims, pointing to a succession of growth increments, with either a large or a low concentration in aluminum, a trace element in quartz. The Al-richer/poorer growth rims contain fluid inclusions that in average record lower/higher fluid pressure, respectively. As a consequence of the correlation between fluid pressure and aluminum content in quartz, the latter signal appears as a new proxy of fluid pressure at depth. It bears the large advantage, with respect to fluid inclusions, not to be affected by reequilibration processes that erase the original message from the depth. The temporal variations in aluminum/fluid pressure are interpreted as the result of the seismic cycle.

1. Introduction

Pore fluid pressure in rocks is an essential parameter in the dynamics of subduction zones, yet one of the most difficult to quantify at seismogenic depth. For instance, as predicted by the critical taper theory of accretionary wedges (Dahlen, 1990), the fluid pressure field controls the general architecture of wedges and the distribution of the fault zones they contain (Mourgues & Cobbold, 2006). During seismic slip, fluid pressure is also involved in dynamic feedback processes that influence the behavior of the principal slip zone of faults (Rice, 2006). In the post-seismic stage, coseismic fracturing modifies the fluid pressure over a large volume of rock surrounding faults (the so-called fault-valve model of Sibson (1994)), which in turn may impact the location and magnitude of aftershocks. More generally, the level of fluid pressure, as inferred from V_p/V_s ratios, seems to be a major control on the seismic versus aseismic character of the plate interface in subduction zones (Audet & Schwartz, 2013; Moreno et al., 2014). Below the downdip limit of the seismogenic zone, high fluid pressure coincides broadly with the location of deep episodic tremor and slip (ETS) events (Audet & Kim, 2016).

15252027, 2022, 10, Downloaded from https://agupubs.onlinelibrary.wiley.com/doi/10.1029/2022GC010346 by Portail BibCNRS INSU, Wiley Online Library on [12/10/2022]. See the Terms and Conditions (https://onlinelibrary.wiley.com/terms-and-conditions) on Wiley Online Library for rules of use; OA articles are governed by the applicable Creative Commons License

For all these reasons, decades of research have been devoted to the determination of spatial and temporal fluid pressure variations in subduction zones. At depths greater than a few kilometers, fluid pressure can only be estimated via indirect methods such as seismic tomography (Kodaira et al., 2004), or from the study of exhumed rocks from ancient subduction zones. In this second category, fluid inclusions, which represent true samples of fluids trapped at depth in minerals, have been widely used as a proxy to estimate the pore pressure in deforming rocks. Several fluid inclusion studies focused on tectonic areas have concluded to the existence of large pressure variations up to ~200 MPa (Berger & Herwegh, 2019; Herrington & Wilkinson, 1993; Mullis, 1979, 1988; Robert et al., 1995; Vrojlik, 1987; Weatherley & Wenley, 2013; Wilkinson & Johnston, 1996), on the basis of large ranges in fluid isochores or unmixing of fluids as a result of sudden pressure drops.

Despite these successes, the use of fluid inclusions as proxies for fluid pressure suffers severe limitations, because of possible post-entrapment reequilibration during exhumation. Aqueous fluid inclusions are particularly prone to such reequilibration because of (a) the solvent action of water on many host minerals (Bodnar, 2003), leading to dissolution-precipitation of inclusion walls (Lambrecht & Diamond, 2014), (b) leakage by diffusion of H_2O from the cavity (Hall & Sterner, 1993; Vityk et al., 2000), or (iii) plastic deformation of the cavity wall enhanced by hydrolitic weakening (Vityk et al., 2000). As a result, the fluid pressure reconstructed from fluid inclusion properties is in many cases modified after entrapment, especially in exhumed accretionary prisms (Raimbourg et al., 2018). Additional tools would thus be extremely valuable to supplement or replace fluid inclusions as proxies for fluid pressure and its changes in time in exhumed rocks.

The purpose of this work is to propose an alternative and complementary approach to investigate fluid pressure variations in deformed and exhumed rocks, relying not only on fluid inclusions but also on the trace element chemistry of their host crystal. Hydrothermal quartz veins with growth zoning is a microstructure that formed contemporaneously with brittle deformation (T < 300°C) in accreted sediments (Mullis, 1975; Raimbourg et al., 2018, 2021; Vrojlik, 1987). Taking exhumed veins from the paleo-accretionary prism of southwestern Japan as examples, we jointly measured the pore pressure record of methane-rich fluid inclusions (much less prone to reequilibration than H_2O-rich inclusions (Vityk & Bodnar, 1995a; Vityk et al., 1994)) and the trace-element composition of their host quartz. Our results suggest that quartz trace element chemistry is sensitive to pore pressure variations, which may provide a new tool to quantitatively estimate fluid pressure in exhumed rocks.

2. Sample Selection and Results

Three hydrothermal quartz vein samples from an exhumed accretionary prism were selected for a joint analysis of fluid inclusions and trace element compositions (Table S2 in Supporting Information S1). The three veins come from strongly deformed rocks near major fault zones belonging to the Shimanto Belt in Japan and constitute either the core of faults/shear bands, or mode I tension cracks formed in the vicinity of faults/shear bands. Quartz veins are considered in all three examples as the result of silica precipitation from water filling the deformation structures.

The Shimanto Belt is a paleo-accretionary prism located landward from the modern subduction margin bordering SW Japan (Taira et al., 1988). Sample 2018NOB2-grain2 comes from top-to-the-SE, meter-scale faults in the Coherent Hyuga, in the footwall of the Oyabu Thrust (Imai et al., 1975). Sample NB25_46 comes from quartz veins in the Hyuga Tectonic Mélange, in the footwall of the Nobeoka Tectonic Line (NTL), a major fault on Kyushu Island, exposed along the eastern coast, near the city of Nobeoka (Murata, 1997). Sample HN441A comes from a shear band in the upper section of the Mugi Mélange, on the island of Shikoku, and is located close to the Minami-Awa fault, the mélange roof thrust (Ikesawa et al., 2005). Both the NTL and Minami-Awa faults contain in their cores layers interpreted as pseudotachylytes formed during seismic slip (Hasegawa et al., 2019; Ujiie et al., 2007).

All three vein samples are kinematically consistent with the top-to-the-SE shear deformation prevalent in their host mélange, interpreted as reflecting deformation along the plate interface as well as within the accretionary prism (Raimbourg et al., 2014, 2017, 2019). Such deformation resulted in horizontal shortening and burial, hence presumably coincided with the peak in pressure-temperature conditions. We therefore assign the growth of the veins considered here to the peak in temperature conditions, as determined by Raman Spectra of Carbonaceous Material (RSCM) around 210°C for the three samples (Table S1 in Supporting Information S1).

10.1029/2022GC010346

15252027, 2022, 10, Downloaded from https://agupubs.onlinelibrary.wiley.com/doi/10.1029/2022GC010346 by Portail BibCNRS INSU, Wiley Online Library on [12/10/2022]. See the Terms and Conditions (https://onlinelibrary.wiley.com/terms-and-conditions) on Wiley Online Library for rules of use; OA articles are governed by the applicable Creative Commons License

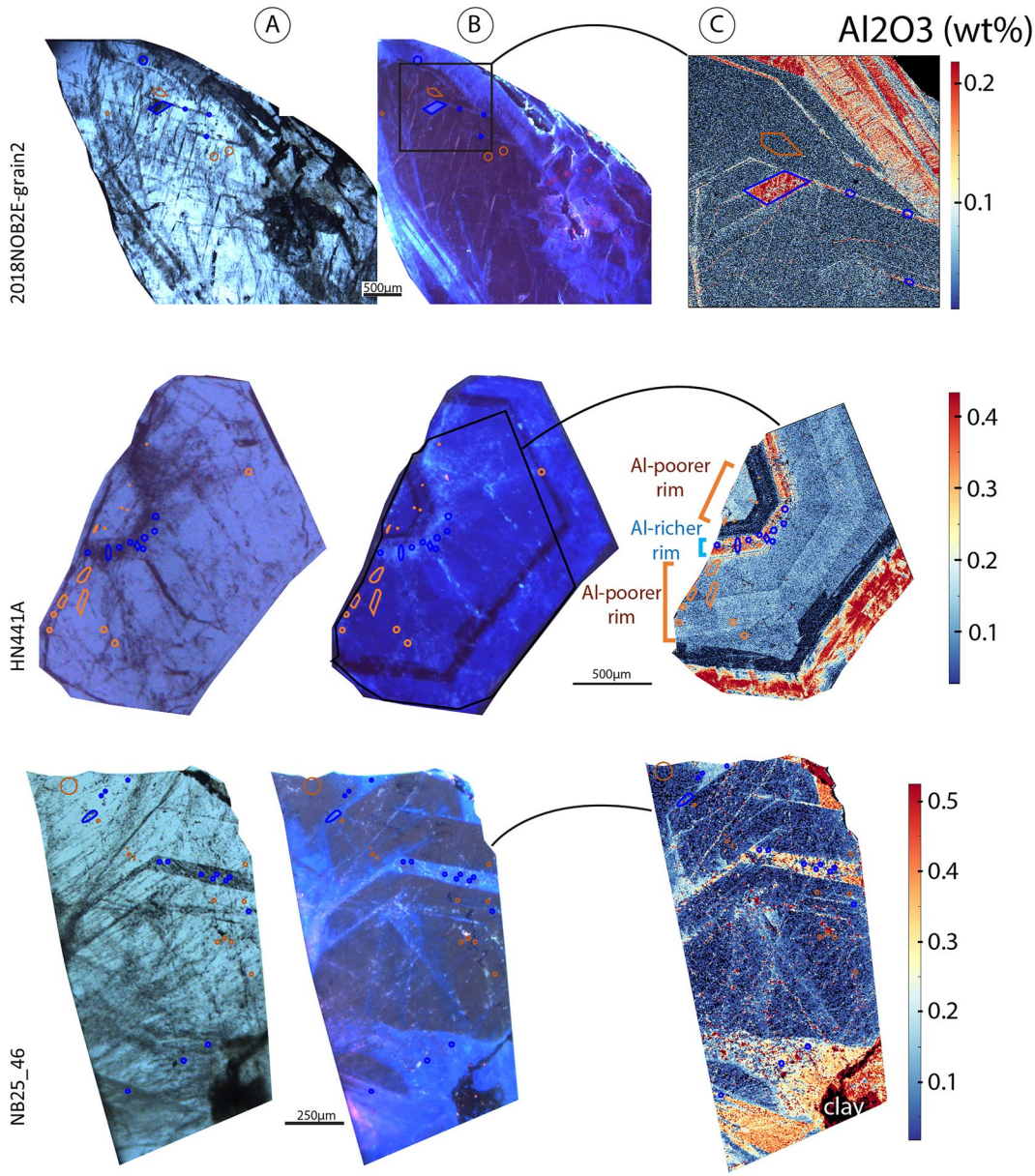


Figure 1. Quartz crystals showing growth rims microstructures in deformation veins from the Shimanto Belt, Japan (HN441A, top; 2018NOB2E_grain2, middle; NB25_46, bottom). (a) Optical microscope pictures (where blue and brown outlines refer to the methane-rich fluid inclusions analyzed and associated with cathodoluminescence (CL)-blue and CL-brown quartz, respectively), (b) cathodoluminescence (CL) images, and (c) electron probe micro-analysis maps of Al concentration. Contrasts in luminescence underline growth structures (as well as fractures in bottom sample), with alternating rims of bright blue luminescence and dark brown luminescence. The domains of quartz with bright CL-blue colors have also a much higher abundance of fluid inclusions than CL-brown domains. Bright CL-blue domains have also a systematically higher Al concentration than dark CL-brown rims.

These samples were selected based on two criteria. The first criterion is the presence of growth rims in quartz, attesting to changes in thermodynamic conditions during precipitation-induced crystal growth. The three vein samples contain elongated quartz crystals, some of them up to 1 cm-long, with faceted terminations toward the core of the vein. The growth rims follow the crystallographic orientations of euhedral quartz (Figure 1). Under cathodoluminescence (CL), growth rims appear as alternating bright blue and dark brown colors.

As a second criterion, the quartz vein samples were selected for their abundant content in methane-rich fluid inclusions. Most of them are primary (i.e., trapped during crystal growth), as their distribution follows the growth

15252027, 2022, 10, Downloaded from https://agupubs.onlinelibrary.wiley.com/doi/10.1029/2022GC010346 by Portail BibCNRS INSU, Wiley Online Library on [12/10/2022]. See the Terms and Conditions (https://onlinelibrary.wiley.com/terms-and-conditions) on Wiley Online Library for rules of use; OA articles are governed by the applicable Creative Commons License

rim patterns of quartz. Only these methane-rich fluid inclusions were considered in the present study in order to minimize the bias of post-entrapment reequilibration that often affects H_2O-rich fluid inclusions (Vityk & Bodnar, 1995a; Vityk et al., 1994). Methane-rich fluid inclusions have sizes that vary from ~1 μm to a few microns (Figure S1 in Supporting Information S1).

We analyzed with Raman spectroscopy the gas phase in the methane-rich fluid inclusions trapped within quartz growth rims in order to reconstruct their trapping pressure (Mullis, 1979). The position of the sharp Raman peak of methane depends on the density of the fluid inclusion (Text S1 in Supporting Information S1). In turn, the density of the fluid inclusions at ambient temperature can be used to compute an isochoric line in P-T space. The pressure of trapping may then be deduced by projecting the temperature of trapping, if known, onto the isochoric line. To do so, we used the aforementioned host rock peak temperature of 210°C, which is assumed to represent the trapping temperature of the fluid inclusions. In the three examples analyzed and irrespective of the CL-color of quartz, the distribution of density is relatively wide, pointing to relative variable conditions of fluid pressure in space and time (Figure 2). Nevertheless, in all three examples, CL-blue quartz rims contain fluid inclusions with lower density values than those in CL-brown quartz rims, as reflected in the decrease in median and average density. After computation of trapping pressures from isochoric lines, for each example, the median pressure is shifted toward lower values in CL-blue quartz rims than in CL-brown rims (Figure 3). The shift is significant, from ~25 to ~70 MPa, depending on the sample, and larger than the uncertainty in measurements (Text S1 in Supporting Information S1).

In tandem with the fluid inclusion analysis, the trace element chemistry of quartz within growth rims was constrained quantitatively with electron probe micro-analysis (EPMA) mapping (Text S1 in Supporting Information S1). These maps reveal that CL-blue growth rims have systematically higher Al_2O_3 concentrations than CL-brown rims. CL-blue rims thus correspond not only to lower trapping pressures of fluid inclusions but also to higher incorporation of Al in quartz than CL-brown rims. The differences between CL-blue and CL-brown rims amount to 0.18, 0.21 and 0.28 wt% in the three samples (Figure 3). Furthermore, across the three samples, the difference in median Al_2O_3 concentration between the two types of growth rims correlates with the difference in median pressure recorded in the fluid inclusions. In other words, larger fluid pressure variations are correlated with larger variations in Al concentration during crystal growth.

3. Discussion

The systematic difference in fluid inclusion densities in growth rims from the three samples attest to fluid pressure fluctuations during quartz precipitation, vein development, and deformation of the Japanese accretionary prism. CL-brown quartz rims crystallize at higher values of fluid pressure whereas CL-blue quartz rims are related to fluid pressure drops (Figure 4).

We suggest that such fluid pressure fluctuations are responsible for the contrasted CL colors and their variations in Al concentration. Indeed, crystal zoning during mineral precipitation from a melt or an aqueous solution has been interpreted as being controlled to a large extent by the rate of crystal growth (Merinero et al., 2009; Welsch et al., 2013, 2014). Fluid pressure drop leads to high silica oversaturation and elevated growth rate. In turn, rapid crystal growth is accompanied by a higher incorporation of impurities, such as fluid inclusions, Al and Li (Ihinger & Zink, 2000), and by a bright and blue cathodoluminescence. With time, the subsequent recovery of higher fluid pressure reduces the supersaturation of Si and the crystal growth rate. Accordingly, in this stage, a slower growth results in fewer substitutions of Si by Al and other trace elements (in particular the charge-compensating Li, for example, Raimbourg et al. (2021)), yielding rims of dark brown quartz under CL.

Similarly to the present study, cyclical patterns of growth have already been described in vein quartz, either from CL imaging (Wilkinson & Johnston, 1996) or from crack-seal microstructures (Fisher & Brantley, 2014; Ramsay, 1980). In addition, models of rapid quartz growth in veins due to fluid pressure drops have also been proposed (Berger & Herwegh, 2019; Weatherley & Wenley, 2013) and supported by fluid inclusion data (Robert et al., 1995; Vrojlik, 1987; Wilkinson & Johnston, 1996). Nonetheless, the present work is the first to tie all these elements together and to demonstrate that growth rims in quartz veins and their CL colors, fluctuating fluid inclusion abundances, and Al-zoning can all be explained by variations in fluid pressure during syn-deformation vein development.

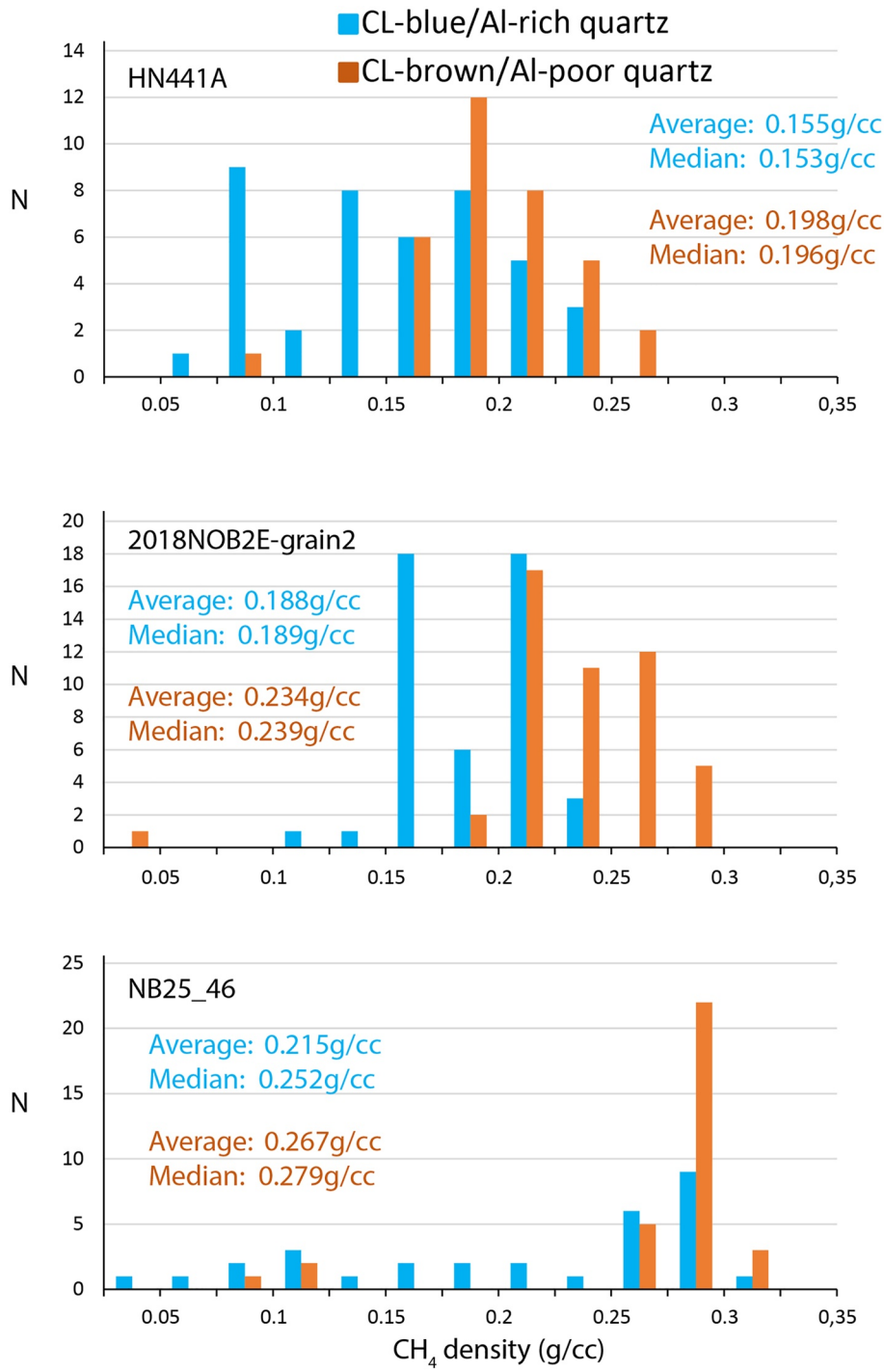


Figure 2. Density histogram of the methane contained in methane-rich fluid inclusions, with a coloring that depends on the cathodoluminescence (CL)-brown or CL-blue domain of host quartz the inclusions belong to. The methane-filled fluid inclusions measured are shown as outlines in Figure 1.

The control by a single process explains the quantitative correlation between the amplitude of the fluid pressure drop recorded by fluid inclusions and the variations in Al concentration in quartz rims (Figure 3). The consequence of this correlation in Figure 3 is that Al concentration in quartz may be considered as a new tool to quantitatively constrain fluid pressure variations during vein development. Considering that the three studied samples come from strongly deformed rocks near major faults, such fluid pressure variations in time are likely related to

15252027, 2022, 10, Downloaded from https://agupubs.onlinelibrary.wiley.com/doi/10.1029/2022GC010346 by Portail BibCNRS INSU, Wiley Online Library on [12/10/2022]. See the Terms and Conditions (https://onlinelibrary.wiley.com/terms-and-conditions) on Wiley Online Library for rules of use; OA articles are governed by the applicable Creative Commons License

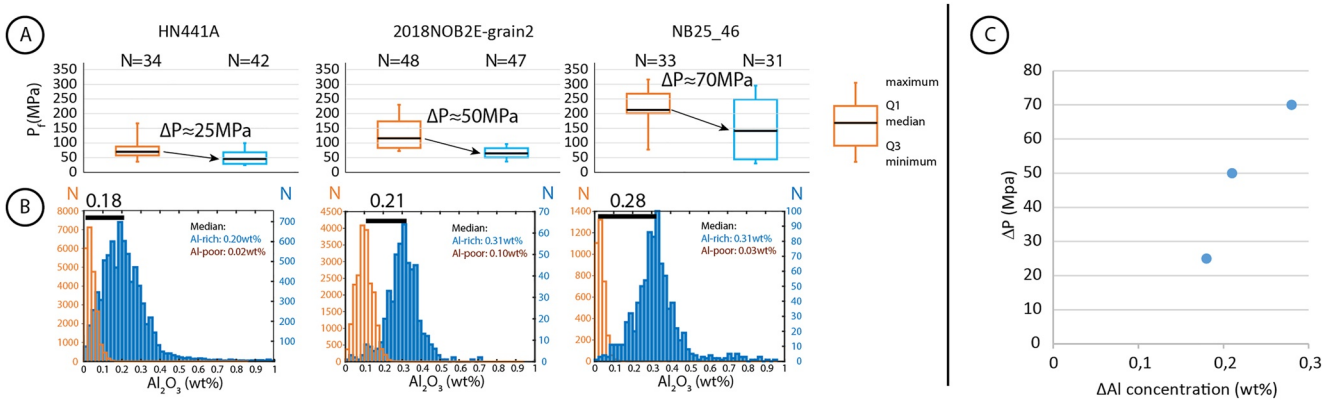


Figure 3. (a) Distribution of pressure for the inclusions from the three samples, extrapolated from inclusion density measured by Raman spectroscopy assuming $T = 210°C$. The ΔP between cathodoluminescence (CL)-brown and CL-blue is estimated from the differences in median values. Q1 and Q3 stand for the values of the first and third quartile of the distribution. (b) Distribution of Al concentration (in correspondence with (A)), processed from EPMA maps using XMapTools (Lanari et al., 2014, 2019), where one analysis corresponds to one pixel in the EPMA map. The difference in Al concentration (ΔAl) between CL-brown and CL-blue domains is estimated as the difference between the modes of the distribution. (b) Plot of ΔP as a function of ΔAl for the three samples analyzed.

earthquakes, as proposed in models of the seismic cycle (Sibson, 1994). If so, the growth rims, with their contrast in trace element chemistry and growth conditions, are therefore a time record of the fluid pressure evolution during the succession of earthquakes and seismic cycles (Figure 4).

The amount of silica precipitated by a 25–70 MPa fluid pressure drop can be estimated (Text S2 in Supporting Information S1), following the approach Berger and Herwegh (2019) proposed to account for the formation of zoned quartz overgrowth (cockades) in alpine fault zones. In cockades as in the present study, the local amount

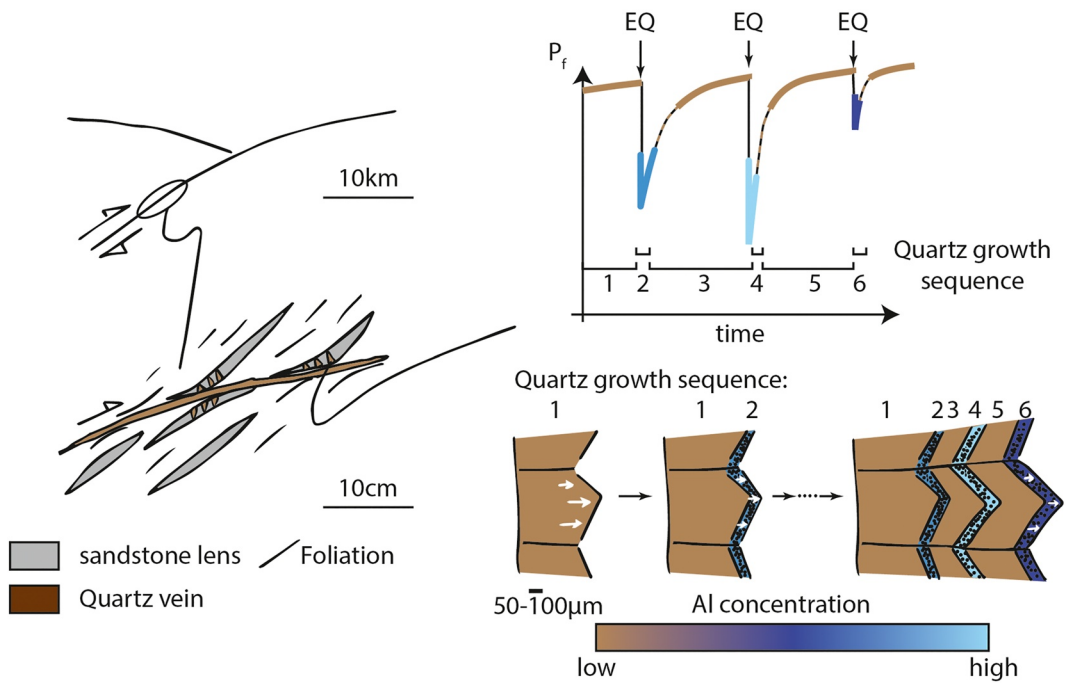


Figure 4. Model of the record by quartz trace element chemistry of fluid pressure evolution during a seismic cycle. Quartz veins grow in shear bands and mode I cracks compatible with the kinematics of the convergent zone. The growth results from repetitions of two-staged sequences, which follow the fluid pressure evolution. During the interseismic period, the pressure is high, the quartz growth is slow and the crystals incorporate few fluid inclusions and a small concentration of Al. In contrast, during or just after the large fluid pressure drop that follows earthquakes (« EQ »), the quartz growth is rapid and the crystals incorporate abundant fluid inclusions and a large concentration of Al that scales with the amplitude of the fluid pressure drop.

15252027, 2022, 10, Downloaded from https://agupubs.onlinelibrary.wiley.com/doi/10.1029/2022GC010346 by Portail BibCNRS INSU, Wiley Online Library on [12/10/2022]. See the Terms and Conditions (https://onlinelibrary.wiley.com/terms-and-conditions) on Wiley Online Library for rules of use; OA articles are governed by the applicable Creative Commons License

15252027, 2022, 10, Downloaded from https://agupubs.onlinelibrary.wiley.com/doi/10.1029/2022GC010346 by Portail BibCNRS INSU, Wiley Online Library on [12/10/2022]. See the Terms and Conditions (https://onlinelibrary.wiley.com/terms-and-conditions) on Wiley Online Library for rules of use; OA articles are governed by the applicable Creative Commons License

of dissolved silica present in the water filling the fault is not sufficient for the overgrowth to be formed. A flow of low pressure, silica-oversaturated water is required in the fault core to provide the necessary silica, probably over short (i.e., minute) time-scales as inferred in Berger and Herwegh (2019).

Each of the six populations of fluid inclusions encompasses a large range of fluid pressures (Figure 3). The reasons for this large range are multifold. One reason is intrinsic to the fluid inclusion record, and results from the fact that, even within a single growth domain of quartz, fluid inclusions are trapped diachronously during fluid pressure variations. Then, there are extrinsic reasons for the fluid inclusion population to record varying pressures: (a) Post-entrapment modifications of fluid inclusions, even methane-rich, cannot be ruled out (Bodnar, 2003; Vityk & Bodnar, 1995a, 1995b; Vityk et al., 1994), these modifications being in some cases impossible to detect by optical microscopy (Mercury et al., 2021); (b) in the quartz veins considered, fluid inclusions are so abundant that some of them might be secondary, despite our effort to avoid them. For these extrinsic reasons, we believe that considering statistical variables such as average or median values, rather than all individual data points in the distribution, is a more robust analysis.

The amplitude of pressure variations at seismogenic depth recorded in our samples from a Japanese accretionary prism is in the range 25–70 MPa, similar to or slightly lower than previous estimates from fluid inclusion studies in similar settings (Herrington & Wilkinson, 1993; Mullis, 1979, 1988; Robert et al., 1995; Vrojlik, 1987). Yet, the amplitude of stress drops after large earthquakes, as inferred from focal mechanisms (Hardebeck, 2012; Hasegawa et al., 2012) or borehole breakouts (Lin et al., 2013), is at most of the order of 10–15 MPa. Our estimate of fluid pressure variations during earthquake cycles thus remains significantly higher than the stress drop obtained from geophysical studies. This difference supports the fault-valve model by Sibson (1994), where the fluid pressure variations are related to the breaching of impermeable barriers by a seismic rupture, rather than the local stress release in the rocks surrounding a slipping fault. The fault-valve model thus provides a viable mechanism to explain the transport of silica-supersaturated fluids required for the fast growth of CL-blue quartz rims.

The conclusion of our study is that CL imaging and EPMA mapping of syn-tectonic quartz appears as a powerful marker of fluid pressure changes during seismic deformation (Figure 4). The luminescence cannot yet be used as a quantitative tool, but Al concentration variations in quartz may provide a quantitative way to assess the fluid pressure fluctuations. Assessing the trace element chemistry of quartz is much easier and accessible than microthermometry; it is applicable to any vein, even those devoid of fluid inclusion. In addition, geochemical zoning and associated luminescence is a signal resistant to post-entrapment alteration, as the low temperature of the vein quartz considered prevents any significant solid-state diffusion of the trace elements responsible for the luminescence. Unlike fluid inclusions, prone to reequilibrate after entrapment, the conditions of the deeply trapped fluid are frozen in the composition of the growth rims as long as Al does not diffuse in quartz (i.e., below ~650°C (Tailby et al., 2018)). Growth rims are a very common feature of quartz crystals formed at low temperature (below 300–350°C), described in many exhumed convergent zones (Jourdan et al., 2009; Raimbourg et al., 2018, 2021; Ramseyer & Mullis, 1990). Aluminum mapping of syn-tectonic quartz veins highlighted in our work offers a promising tool to quantitatively constrain fluid pressure variations in exhumed settings, and especially to further understand earthquake processes in convergent zones. Further progresses require hydrothermal experiments of quartz growth (for example, Okamoto et al. (2010)) aimed at quantitatively constraining the relationship between fluid pressure variation, oversaturation of the solution and uptake of Al in the growing crystal.

Data Availability Statement

The data used in this study are available at https://doi.org/10.26022/IEDA/112290.

Acknowledgments
The authors acknowledge support from both LabEx VOLTAIRE (ANR-10-LABX-100-01) and EquipEx PLANEX (ANR-11-EQPX-0036) projects. Calculations of the thermodynamic properties of water were carried out using the platform at: https://calcul-isto.cnrs-orleans.fr/calisto/property/.

References

Audet, P., & Kim, Y. (2016). Teleseismic constraints on the geological environment of deep episodic slow earthquakes in subduction zone forearcs: A review. *Tectonophysics*, *670*, 1–15. https://doi.org/10.1016/j.tecto.2016.01.005

Audet, P., & Schwartz, S. Y. (2013). Hydrologic control of forearc strength and seismicity in the Costa Rican subduction zone. *Nature Geoscience*, *6*(10), 852–855. https://doi.org/10.1038/ngeo1927

Berger, A., & Herwegh, M. (2019). Cockade structures as a paleo-earthquake proxy in upper crustal hydrothermal systems. *Scientific Reports*, *9*(1), 9209–9217. https://doi.org/10.1038/s41598-019-45488-2

Bodnar, R. J. (2003). Reequilibration of fluid inclusions. In A. Anderson, & D. Marshall (Eds.), *Fluid inclusions: Analysis and interpretation* (Vol. 32, pp. 213–230). Mineralogical Association of Canada. Short Course.

Dahlen, F. A. (1990). Critical taper model of fold-and-thrust belts and accretionary wedges. *Annual Review of Earth and Planetary Sciences*, *18*(1), 55–99. https://doi.org/10.1146/annurev.ea.18.050190.000415
Fisher, D. M., & Brantley, S. L. (2014). The role of silica redistribution in the evolution of slip instabilities along subduction interfaces: Constraints from the Kodiak accretionary complex, Alaska. *Journal of Structural Geology*, *69B*, 395–414. https://doi.org/10.1016/j.jsg.2014.03.010
Hall, D. L., & Sterner, S. M. (1993). Preferential water loss from synthetic fluid inclusions. *Contributions to Mineralogy and Petrology*, *114*(4), 489–500. https://doi.org/10.1007/bf00321753
Hardebeck, J. L. (2012). Coseismic and postseismic stress rotations due to great subduction zone earthquakes. *Geophysical Research Letters*, *39*(21), 1–6. https://doi.org/10.1029/2012gl053438
Hasegawa, A., Yoshida, K., Asano, Y., Okada, T., Iinuma, T., & Ito, Y. (2012). Change in stress field after the 2011 great Tohoku-Oki earthquake. *Earth and Planetary Science Letters*, *355–356*, 231–243. https://doi.org/10.1016/j.epsl.2012.08.042
Hasegawa, R., Yamaguchi, A., Fukuchi, R., Hamada, Y., Ogawa, N., Kitamura, Y., et al. (2019). Postseismic fluid discharge chemically recorded in altered pseudotachylyte discovered from an ancient megasplay fault: An example from the Nobeoka thrust in the Shimanto accretionary complex, SW Japan. *Progress in Earth and Planetary Science*, *6*(6), 1–16. https://doi.org/10.1186/s40645-019-0281-2
Herrington, R., & Wilkinson, J. J. (1993). Colloidal gold and silica in mesothermal vein systems. *Geology*, *21*(6), 539–542. https://doi.org/10.1130/0091-7613(1993)021<0539:cgasim>2.3.co;2
Ihinger, P. D., & Zink, S. I. (2000). Determination of relative growth rates of natural quartz crystals. *Nature*, *404*(6780), 865–869. https://doi.org/10.1038/35009091
Ikesawa, E., Kimura, G., Sato, K., Ikehara-Ohmori, K., Kitamura, Y., Yamaguchi, A., et al. (2005). Tectonic incorporation of the upper part of oceanic crust to overriding plate of a convergent margin: An example from the Cretaceous-early Tertiary Mugi Melange, the Shimanto Belt, Japan. *Tectonophysics*, *401*(3–4), 217–230. https://doi.org/10.1016/j.tecto.2005.01.005
Imai, I., Teraoka, Y., Okumura, K., & Ono, K. (1975). *Geological map of Japan, 1:50,000: Mikado*. Geological Survey of Japan.
Jourdan, A.-L., Vennemann, T. W., Müllis, J., Ramseyer, K., & Spiers, C. J. (2009). Evidence of growth and sector zoning in hydrothermal quartz from Alpine veins. *European Journal of Mineralogy*, *21*(1), 219–231. https://doi.org/10.1127/0935-1221/2009/0021-1881
Kodaira, S., Iidaka, T., Kato, A., Park, J. O., Iwasaki, T., & Kaneda, Y. (2004). High pore fluid pressure may cause silent slip in the Nankai Trough. *Science*, *304*(5675), 1295–1298. https://doi.org/10.1126/science.1096535
Lambrecht, G., & Diamond, L. W. (2014). Morphological ripening of fluid inclusions and coupled zone-refining in quartz crystals revealed by cathodoluminescence imaging: Implications for CL-petrography, fluid inclusion analysis and trace-element geothermometry. *Geochimica et Cosmochimica Acta*, *141*, 381–406. https://doi.org/10.1016/j.gca.2014.06.036
Lanari, P., Vho, A., Bovay, T., Airaghi, L., & Centrella, S. (2019). *Quantitative Compositional Mapping of Mineral Phases by Electron Probe Micro-analyser* (Vol. 478(1), pp. 39–63). Geological Society of London, Special Publications. https://doi.org/10.1144/sp478.4
Lanari, P., Vidal, O., De Andrade, V., Dubacq, B., Lewin, E., Grosch, E., & Schwartz, S. (2014). XMapTools: A MATLAB©-based program for electron microprobe X-ray image processing and geothermobarometry. *Computers & Geosciences*, *62*, 227–240. https://doi.org/10.1016/j.cageo.2013.08.010
Lin, W., Conin, M., Moore, J. C., Chester, F. M., Nakamura, Y., Mori, J., et al. (2013). Stress state in the largest displacement area of the 2011 Tohoku-Oki earthquake. *Science*, *339*(6120), 687–690. https://doi.org/10.1126/science.1229379
Mercury, L., De Bilbao, E., Simon, P., Raimbourg, H., Bergonzi, I., Hulin, C., et al. (2021). Quartz stressing and fracturing by pore pressure dropping down to negative pressure. *ACS Earth and Space Chemistry*, *5*, 170–185.
Merinero, R., Lunar, R., Somoza, L., Diaz-del-Rio, V., & Martinez-Frias, J. (2009). Nucleation, growth and oxidation of framboidal pyrite associated with hydrocarbon-derived submarine chimneys: Lessons learned from the Gulf of Cadiz. *European Journal of Mineralogy*, *21*(5), 947–961. https://doi.org/10.1127/0935-1221/2009/0021-1956
Moreno, M., Haberland, C., Oncken, O., Rietbrock, A., Angiboust, S., & Heidbach, O. (2014). Locking of the Chile subduction zone controlled by fluid pressure before the 2010 earthquake. *Nature Geoscience*, *7*(4), 292–296. https://doi.org/10.1038/ngeo2102
Mourgues, R., & Cobbold, P. R. (2006). Thrust wedges and fluid overpressures: Sandbox models involving pore fluids. *Journal of Geophysical Research*, *111*(B05404), 1–15. https://doi.org/10.1029/2004jb003441
Mullis, J. (1975). Growth conditions of quartz crystals from Val d'Illiez (Valais, Switzerland): Schweiz. *Mineralogische und Petrographische Mitteilungen*, *55*, 419–429.
Mullis, J. (1979). The system methane-water as a geological thermometer and barometer from the external part of the Central Alps. *Bulletin de Mineralogie*, *102*(5), 526–536. https://doi.org/10.3406/bulmi.1979.7301
Mullis, J. (1988). Rapid subsidence and upthrusting in the Northern Apennines, deduced by fluid inclusion studies in quartz crystals from Porretta Terme. *Schweizerische mineralogische und petrographische Mitteilungen*, *68*(2), 157–170.
Murata, A. (1997). *Geological map of Miyazaki prefecture, 1:200,000*. Miyazaki Prefectural Government.
Okamoto, A., Saishi, H., Hirano, S., & Tsuchiya, N. (2010). Mineralogical and textural variation of silica minerals in hydrothermal flow-through experiments: Implications for quartz vein formation. *Geochimica et Cosmochimica Acta*, *74*(13), 3692–3706. https://doi.org/10.1016/j.gca.2010.03.031
Raimbourg, H., Augier, R., Famin, V., Gadenne, L., Palazzin, G., Yamaguchi, A., & Kimura, G. (2014). Long-term evolution of an accretionary prism: The case study of the Shimanto Belt. *Kyushu, Japan: Tectonics*, *33*, 1–24.
Raimbourg, H., Famin, V., Palazzin, G., Mayoux, M., Jolivet, L., Ramboz, C., & Yamaguchi, A. (2018). Fluid properties and dynamics along the seismogenic plate interface. *Geosphere: Subduction top to bottom*, *14*(2), 1–23. https://doi.org/10.1130/ges01504.1
Raimbourg, H., Famin, V., Palazzin, G., Sakaguchi, A., Yamaguchi, A., & Augier, R. (2017). Tertiary evolution of the Shimanto Belt (Japan): A large-scale collision in early miocene. *Tectonics*, *36*(7), 1–21. https://doi.org/10.1002/2017tc004529
Raimbourg, H., Famin, V., Palazzin, G., Yamaguchi, A., Augier, R., Kitamura, Y., & Sakaguchi, A. (2019). Distributed deformation along the subduction plate interface: The role of tectonic mélanges. *Lithos*, *334–335*, 69–87. https://doi.org/10.1016/j.lithos.2019.01.033
Raimbourg, H., Rajic, K., Famin, V., Moris-Muttoni, B., Palazzin, G., Fisher, D. M., et al. (2021). Quartz vein geochemistry records deformation processes in convergent zones. *Geochemistry, Geophysics, Geosystems*, *22*(4), 1–35. https://doi.org/10.1029/2020gc009201
Ramsay, J. G. (1980). The crack-seal mechanism of rock deformation. *Nature*, *284*(5752), 135–139. https://doi.org/10.1038/284135a0
Ramseyer, K., & Mullis, J. (1990). Factors influencing short-lived blue cathodoluminescence of α-quartz. *American Mineralogist*, *75*, 791–800.
Rice, J. R. (2006). Heating and weakening of faults during earthquake slip. *Journal of Geophysical Research*, *111*(B05311), 1–29. https://doi.org/10.1029/2005jb004006
Robert, F., Boullier, A. M., & Firdaous, K. (1995). Gold-quartz veins in metamorphic terranes and their bearing on the role of fluids in faulting. *Journal of Geophysical Research*, *100*(B7), 12861–12879. https://doi.org/10.1029/95jb00190
Sibson, R. H. (1994). *Crustal Stress, Faulting and Fluid Flow* (Vol. 78, pp. 69–84). Special Publications of the Geological society of London. https://doi.org/10.1144/gsl.sp.1994.078.01.07

15252027, 2022, 10, Downloaded from https://agupubs.onlinelibrary.wiley.com/doi/10.1029/2022GC010346 by Portail BibCNRS INSU, Wiley Online Library on [12/10/2022]. See the Terms and Conditions (https://onlinelibrary.wiley.com/terms-and-conditions) on Wiley Online Library for rules of use; OA articles are governed by the applicable Creative Commons License

Tailby, N. D., Cherniak, D. J., & Bruce Watson, E. (2018). Al diffusion in quartz. *American Mineralogist*, *103*(6), 839–847. https://doi.org/10.2138/am-2018-5613

Taira, A., Katto, J., Tashiro, M., Okamura, M., & Kodama, K. (1988). The Shimanto Belt in Shikoku, Japan-evolution of cretaceous to miocene accretionary prism. *Modern Geology*, *12*, 5–46.

Ujiie, K., Yamaguchi, H., Sakaguchi, A., & Toh, S. (2007). Pseudotachylytes in an ancient accretionary complex and implications for melt lubrication during subduction zone earthquakes. *Journal of Structural Geology*, *29*(4), 599–613. https://doi.org/10.1016/j.jsg.2006.10.012

Vityk, M. O., & Bodnar, R. J. (1995a). Do fluid inclusions in high-grade metamorphic terranes preserve peak metamorphic density during retrograde decompression? *American Mineralogist*, *80*, 641–644.

Vityk, M. O., & Bodnar, R. J. (1995b). Textural evolution of synthetic fluid inclusions in quartz during reequilibration, with applications to tectonic reconstruction. *Contributions to Mineralogy and Petrology*, *121*(3), 309–323. https://doi.org/10.1007/bf02688246

Vityk, M. O., Bodnar, R. J., & Doukhan, J. C. (2000). Synthetic fluid inclusions. XV. TEM investigation of plastic flow associated with reequilibration of fluid inclusions in natural quartz. *Contributions to Mineralogy and Petrology*, *139*(3), 285–297. https://doi.org/10.1007/s004100000142

Vityk, M. O., Bodnar, R. J., & Schmidt, C. S. (1994). Fluid inclusions as tectonothermobarometers: Relation between pressure-temperature history and reequilibration morphology during crustal thickening. *Geology*, *22*(8), 731–734. https://doi.org/10.1130/0091-7613(1994)022<0731:fiatrb>2.3.co;2

Vrojlik, P. (1987). Tectonically-driven fluid flow in the Kodiak accretionary complex, Alaska. *Geology*, *15*, 466–469.

Weatherley, D. K., & Wenley, R. W. (2013). Flash vaporization during earthquakes evidenced by gold deposits. *Nature Geoscience*, *6*(4), 294–298. https://doi.org/10.1038/ngeo1759

Welsch, B., Faure, F., Famin, V., Baronnet, A., & Bachèlery, P. (2013). Dendritic crystallization: A single process for all theTextures of olivine in basalts? *Journal of Petrology*, *54*(3), 539–574. https://doi.org/10.1093/petrology/egs077

Welsch, B., Hammer, J., & Hellebrand, E. (2014). Phosphorus zoning reveals dendritic architecture of olivine. *Geology*, *42*(10), 867–870. https://doi.org/10.1130/g35691.1

Wilkinson, J. J., & Johnston, J. D. (1996). Pressure fluctuations, phase separation, and gold precipitation during seismic fracture propagation. *Geology*, *24*(5), 395–398. https://doi.org/10.1130/0091-7613(1996)024<0395:pfpsag>2.3.co;2

15252027, 2022, 10, Downloaded from https://agupubs.onlinelibrary.wiley.com/doi/10.1029/2022GC010346 by Portail BibCNRS INSU, Wiley Online Library on [12/10/2022]. See the Terms and Conditions (https://onlinelibrary.wiley.com/terms-and-conditions) on Wiley Online Library for rules of use; OA articles are governed by the applicable Creative Commons License